Computational Modeling of a Single-Element Transcranial Focused Ultrasound Transducer for Subthalamic Nucleus Stimulation

Mohammed A. Samoudi[1], Timothy Van Renterghem[1], and Dick Botteldooren[1]

[1] Ghent University, Department of Information Technology, WAVES research group, Ghent, Belgium.

Email: amine.samoudi@ugent.be; Timothy.VanRenterghem@ugent.be

Abstract

Objective. While transcranial focused ultrasound is a very promising neuromodulation technique for its non-invasiveness and high spatial resolution, its application to the human deep brain regions such as the subthalamic nucleus (STN) is relatively new. The objective of this study is to design a simple ultrasound transducer and study the transcranial wave propagation through a highly realistic human head model. The effects of skull morphology and skull and brain tissue properties on the focusing performance and energy deposition must therefore be known. *Approach.* A full-wave finite-difference time-domain simulation platform was used to design and simulate ultrasound radiation from a single-element focused transducer (SEFT) to the subthalamic nucleus. Simulations were performed using the state-of-the-art Multimodal Imaging-based and highly Detailed Anatomical (MIDA) head model. In addition, the impact of changes in sound speed, density, and tissue attenuation coefficients were assessed through a sensitivity analysis. *Main results*. A SEFT model was designed to deliver an intensity of around $100 W/m^2$ to the STN region; 20% of the STN volume was sonicated with at least half of the maximum of the peak intensity and it was predicted that 61.5% of the volume of the beam (above half of the peak intensity) falls inside the STN region. The sensitivity analysis showed that the skull's sound speed is the most influential acoustic parameter, which must be known with less than 1.2% error to obtain an acceptable accuracy in intracranial fields and focusing (for less than 5% error). S*ignificance.* Ultrasound intensity delivery at the STN by a simple single element transducer is possible and could be a promising alternative to complex multi-element phased arrays, or more general, to invasive or less focused (non-acoustic) neuromodulation techniques. Accurate acoustic skull and brain parameters, including detailed skull geometry, are needed to ensure proper targeting in the deep brain region.

Keywords: ultrasonic neuromodulation, transcranial focused ultrasound, deep brain stimulation, full-wave numerical simulations, subthalamic nucleus stimulation.

I. INTRODUCTION

Deep brain stimulation (DBS), repetitive transcranial magnetic stimulation (rTMS) and transcranial direct current stimulation (tDCS) are well-established treatments for multiple neurological diseases and have directly resulted in an increased understanding of deep brain functional neuroanatomy. However, each of these techniques have drawbacks and limitations. DBS, for example, requires a surgical procedure to implant lead electrodes in the subcortical nuclei of the brain, causing risk of immune response and infection [1]. Both rTMS and tDCS suffer from a lack of spatial-specificity and penetrability, required to target a deep-seated brain region [2, 3].

In contrast, transcranial focused ultrasound (tFUS) was shown to be an appealing approach for noninvasive neuromodulation of both cortical tissue and deeper targets in the brain beyond the cortex. Unlike other brain stimulation techniques (DSB, rTMS, and tDCS), tFUS can achieve a higher spatial resolution (in the order of millimeters), and was already used effectively for cortical neuromodulation in animals [4, 5] and humans [6-8]. tFUS was investigated in relation to different applications (brain tumor ablation, blood-brain barrier opening, and neuromodulation) and by acting through thermal and/or non-thermal mechanisms [9]. tFUS at high intensities (peak power levels exceeding 1000 W/cm^2) is able to thermally ablate brain tissues. The latter demands focusing at a small targeted brain region with a high degree of precision [10, 11]. In contrast to high intensity tFUS, low intensities (10-500 mW/cm^2) were shown to be capable of reversibly modulating targeted brain regions. These low intensities are comparable to what is typically used in diagnostic ultrasound (US) examinations [9, 12, 13]. Due to the low intensity required, the devices used for such applications are mainly single-element focused transducers (SEFT), with a narrow beam applied to the skull just above the targeted stimulation area [14, 15]. Compared to multi-element phased transducer arrays (see e.g. [22, 23]), the requirements for the electronics driving such a SEFT are strongly relaxed and thus much less expensive, increasing the availability of such devices and its potentially wide use. For example, Mueller et al. [14] used a custom designed SEFT (frequency of 0.5 MHz, diameter of 30 mm, and a focal length of 30 mm) and Deffieux et al. [15] used different SEFT designs (frequency 0.3-0.7 MHz, diameter of 42-128 mm).

A potentially interesting application of tFUS is to reversibly modulate neuronal activity of the subthalamic nucleus (STN). Subthalamic nucleus deep brain stimulation (STN-DBS) [16], a surgical technique mainly used to treat patients with advanced Parkinson's disease, suffers from many drawbacks associated with the highly invasive nature of the procedure and related risks like infection and hemorrhage [16, 17]. The tFUS technique is thus a potentially interesting non-invasive alternative not altering the target neurons network. Stimulations of the deep brain region have been successfully performed transcranially in various animal species, including mice [18, 19], rats [20], sheep [21], and monkeys [15]. Although these studies suggest possibilities for using ultrasonic waves for human deep brain stimulation, targeting the deep brain regions with ultrasound has been mainly performed for brain tumor ablation using high-intensity large phased arrays of transducers [22, 23]. A main question is whether neurostimulation could be performed with less advanced and more commonly available SEFTs.

Unlike other non-acoustical brain stimulation techniques, ultrasound energy is attenuated and disrupted by the human skull. The skull is the primary barrier to deliver ultrasonic energy to the targeted area, characterized by strong and frequency dependent shielding, absorption, scattering, and refraction of ultrasonic waves. Not only the interfaces encountered (air/water/gel and skull, and skull and brain tissue) will diverge ultrasonic beams, but also the skull itself is acoustically spoken a complex layered medium. It consists of three layers namely the outer and inner tables made of solid bone, and a central layer of diploe consisting of cancellous bone. In contrast to the outer layers, the diploe is characterized by a large and highly frequency-dependent attenuation [24]. The relative thicknesses of the different layers strongly depend on the location along the human head, and there are strong interpersonal differences.

The presence of the human skull will thus result in a significant distortion of the transmitted ultrasound beam. Since the skull of animals is much smaller and thinner than that of humans [18-20], numerical investigation of ultrasonic wave propagation through the much more complex human skull is key to design SEFT transducers to reach a deep brain region such as the STN prior to applications. To the authors' knowledge, no acoustic transducer has been designed or used before to target the STN

aiming at neuromodulation. However, most of the studies investigating the effect of the human skull on the acoustic wave propagation use simplified or human alike head models without detailed tissue structures or skull geometry [6, 7, 14, 15]. Only changing the simplified skull geometry from flat to curved in [14] already lead to a reduction in the peak intensity by 40% in the target area. In addition, in a realistic head model, due to its non-uniformity and variable curvature, the resulting pressure field distribution will be much more sensitive to the transducer position [14]. Recently, Legon et al. [7] tested the ability of a single-element transducer to modulate unilaterally the thalamus in humans by analyzing recorded somatosensory evoked potentials from scalp electrodes. Numerical simulations were performed using the Visible Human Project male to investigate the effect of different skull morphologies for deep brain neuromodulation in humans. Note that the Visible Human male used in [7], compared to the MIDA (Multimodal Imaging-Based Detailed Anatomical) head model [25] that will be used in this work, has less detailed skull layering and brain tissue discrimination.

Recently, Iacono et al. [25] developed such a multimodal anatomical model of the human neck and head. The new high resolution (up to 500 μm) head model contains 153 structures in the head with detailed characterization of the deep brain tissues along with an atlas-based segmentation, making the MIDA model among the most advanced anatomical image-based models. The MIDA skull model comes with three main layers, i.e., outer table, diploe, and the inner table. The skull layers were discriminated using T2-weighted MRI, which enhanced the cancellous bone intensity inside the diploe compared to the cortical bone of the inner and outer tables [25]. Differentiating between these different skull layers is important for the current application of the tFUS modeling.

The objective of this work is to numerically design and investigate an adapted single-element transducer to deposit low-intensity ultrasonic energy in the deep brain, more precisely in the STN region, using a state-of-the-art physical simulation technique and a highly detailed human head model. A sensitivity analysis on reported skull and brain acoustic parameters found in literature will be conducted as well.

II. METHODS

A. *Ultrasound propagation model*

The commercial software package Sim4Life [26] has been used to model the transcranial ultrasound propagation to the STN. Sim4Life is a simulation platform, combining computable human phantoms with advanced physics solvers and tissue models. Full-wave propagation is simulated, based on the Westervelt-Lighthill equation [27], which is essentially a weakly non-linear approximation of the ultrasound propagation physics [28]. This equation was extended with a density variation term to account for the abrupt impedance jumps encountered when propagating through the skull [29]:

$$\rho\nabla.\frac{1}{\rho}\nabla p - \frac{1}{c^2}\frac{\partial^2 p}{\partial t^2} + \frac{\delta}{c^4}\frac{\partial^3 p}{\partial t^3} + \frac{\beta}{2\rho c^4}\frac{\partial^2 p^2}{\partial t^2} = 0 \quad (1)$$

where p denotes the acoustic pressure, c represents the speed of sound, t is time, ρ is mass density, β is the nonlinearity coefficient, and δ is the diffusivity of sound in a thermo-viscous fluid.

The 3D finite-difference time-domain method is used to discretize these continuous equations (see [29] for more details). The fact that this is a volume discretization technique allows for heterogeneous material properties (more precisely speed of sound, medium density, and US attenuation coefficient) to be assigned in high spatial detail. Only longitudinal pressure waves are considered. Since the incident wave fronts, relative to the skull, are close to orthogonal, elastic wave propagation (and the associated shear waves) are of minor importance [24, 30]. The ultrasound propagation module has been well validated before (see e.g. [29]).

B. *Transducer design*

The piezo-electric ultrasound transducer (Fig. 1) used is a custom-designed SEFT having a center frequency of 0.5 MHz. The geometrically focused transducer has a curvature radius of 120 mm and an aperture width of 100 mm. The SEFT transducer design was adapted to provide a focal spot tailored to the STN with a focal length long enough to accommodate this brain structure dimensions with a minimum intensity of 100 W/m^2.

A design frequency of 0.5 MHz is often seen in known applications of tFUS (see literature review in Ref. [31]). At higher frequencies, sufficient transmission through the skull [24, 32] would need high intensity transducers and consequently pronounced absorption and tissue heating risks [33]. Lower sound frequencies, in contrast, might give rise to an increase in the size of the focal spot. In addition, standing waves in the human head will become more pronounced and might lead to insufficient control of the deposited ultrasonic energy, although signal processing techniques have been proposed to limit such effects [34]. At the same time, single element curved transducers are still applicable without the need for phase control [24, 35, 36]. The SEFT was positioned at the side of the head above the ear. This part of the skull, the temporal bone, can be considered an 'acoustic window' since it is the thinnest part of the human skull [14].

C. Anatomical models and acoustical tissue properties

The MIDA human head model (Fig. 2) was first used to investigate the acoustic intensity and pressure distribution in the target area. MIDA is an advanced multimodal imaging-based anatomical model of the human neck and head. This model comes with a large number of 153 high-resolution structures, including several distinct deep brain structures, skull layers and bones, nerves, as well as veins and arteries [25]. The skull was actually modeled as three different layers namely the outer table, inner table, and the diploe. The inner and the outer tables use the same acoustic parameters, while the diploe is slightly different. The sound speed for the inner and the outer tables is equal to 2300 m/s and set to 2013 m/s for the diploe. The density is equal to 1912 kgm^{-3} for the inner and the outer tables and equal to 1740 kg$m^{-3}$for the diploe.

Distinguishing between different deep brain structures is of high relevance for the current study and possible with the MIDA head model. Tissue parameters were set based on literature [37-39].

Table I shows the main material properties of the brain tissues. We modelled a 20-mm water layer between the surface of the SEFT and the human head model. This choice was based on the typical set up used in animal experiments [18-21]. The location of the STN inside the brain is shown in Fig. 3 [25, 40, 41]. Targeted regions of the STN are the side and upper region [16, 17] with a

sonicated volume of 10%-25%. These goals are based on STN-DBS procedures [16, 17] and tFUS deep brain stimulation applications in animals [15, 18, 20].

D. Basic validation of ultrasound propagation in a water tank

A basic validation of the simulation software was performed. A single-element ultrasound transducer was designed to replicate a commercial custom-designed SEFT (Blatek, Inc., State College, PA, USA). The transducer was geometrically focused having a center frequency of 0.5 MHz, a diameter of 30 mm, and a focal length of 30 mm [14]. Results were compared to experimental data and to numerical outcomes using the COMSOL simulation platform as reported in [14]. Free water transmission in the acoustic test tank using this setup resulted in a spatial-peak pulse-average intensity of 23.87 W/cm^2 similar as also reported in [7]. Table II shows the main SEFT parameters used for this validation exercise.

Figure 4.a shows the intensity distribution in the YZ plane through the focus point and along the z-axis ($y \cong 0$). Quantification of the potential stimulation area by the focused ultrasound beam was performed using the region having an intensity greater than the half maximum. This full width at half maximum (FWHM) threshold shows an elliptical profile. Figure 4.b depicts the predicted half maximum intensity profiles using Sim4Life.

Table III shows a more detailed comparison of the FWHM characteristics. Note that the experimental results are characterized by an ultrasound transmission axis slightly misaligned from the vertical in the intensity maps. Most likely, this is due to a positioning error of the ultrasound transducer during mounting in the acoustic tank. The numerical model used in the current work is in good quantitative agreement with the empirical observations (deviation of 8.8% and 0.9% for the maximum pressure and the maximum intensity, respectively) and with the COMSOL computational model (deviation of 0% and 0.9% for the maximum pressure and the maximum intensity, respectively).

E. Parameters considered for evaluating ultrasound energy delivery at the STN

For each modelled case, peak intensity, pressure, and displacement compared with free water propagation are provided. A quantification of the targeting properties are computed as follows. The Target overlap estimates the volume of the STN above the half-intensity threshold; a 100% value indicates the case where the beam encompasses the entire STN volume with an intensity higher than half of the peak intensity. The Beam overlap estimates the percentage of the beam volume above half of the peak intensity that falls inside the STN region. A 100% value thus indicates that the beam does not cover any collateral structures. Values for targeting in water, without the skull, are also provided to quantify the skull aberration effects. Lastly, the lengths of the minor and major axes were computed based on the zone with intensities greater than the half maximum.

F. Sensitivity of the acoustic properties of the skull, brain, and the STN

The sensitivity of the intracranial field to changes in the acoustic properties of the skull, brain (grey and white matter), and the STN was examined. The values of density, sound speed, and the attenuation coefficient assigned to the skull layer, STN, and the brain (grey and white matter) were separately perturbed by a linear variation. For the skull, the maximum variation assigned to the attenuation coefficient and sound speed was ±75% and ±50%, respectively, based on the range of acoustic properties reported in the literature [14, 27, 37-39, 42]. The range of the human skull density was much narrower [42] and reported to be of ±10% of the nominal value used in Table I. A narrower range of ±5% was tested for density, sound speed, and the attenuation coefficient for the STN and the brain [37-39, 42]. Acoustic properties were varied in steps of 1% for the STN and the brain tissues. For the skull, acoustic properties were varied in steps of 2% for the range ±5% (±1, ±3, and ±5) and in steps of 20% beyond that. The reference medium properties assigned to the skull layer, STN and the brain tissues are reported in Table I. Note that for the brain acoustic parameters less extended parameter ranges are needed when analysing literature. This does not hold for the skull acoustic parameters where a much wider range has been reported.

Variation in the intracranial fields due to changes in the tissues' acoustic parameters was quantified relative to the reference simulation. Errors in peak pressure and peak intensity of less than 5% were used as criteria for accurate simulation, based on a previous examination of the parameters

desirable to achieve effective acoustic neurostimulation [41, 43]. We also considered an error of less than 5% for the Target overlap and the Beam overlap as criteria for an accurate focusing.

III. RESULTS

A. Simulation in free water and effect of human skull (MIDA model)

A pressure amplitude of 0.813 kPa on the surface of the transducer was needed to reach an intensity in the targeted region of the STN equal to $100 W/m^2$ in free water. A close-up of computational intensities in the region of focus and characterization of the FWHM intensity profile for the computational model are depicted in Fig. 4.a and Fig. 4.b for simulations in free water. Next, a simulation using the same input pressure and adding the heterogeneous MIDA head model (skull diploe, skull outer table, skull inner table and the brain tissues) was conducted.

Figure 5 shows the acoustic intensity distribution in the MIDA model and a depiction of the FHWM region. Quantification of the different parameters for both configurations is reported in table IV. The peak pressure attenuation through the skull was found to be approximately 56 % compared with that in water; the peak intensity attenuation was evaluated to be 84.9 % compared with that in water. The intensity attenuation of 84.9 % is similar to the percentage found in [14] (81 % using a different design of SEFT at 0.5 MHz). The Target overlap parameter is predicted to be around 23 % (25.4% without the skull) and the Beam overlap parameter is around 36.5% (68.9% without the skull). The peak position was displaced by approximately 1.3 mm (1.3 mm along the beam axis and 0.4 mm in the transverse plane). Then we performed simulations using a slightly adapted SEFT transducer with a pressure amplitude of 2.1 kPa on the surface of the transducer (increase of 260 %) to reach the target value of $100 W/m^2$ in the STN region in the presence of the skull.

Results (Table IV, last column) show that we obtain a larger focused area (26 % greater) in the adjusted model with greater maximum pressure at the STN while losing slightly in terms of the overlapping percentage. The Target overlap parameter for the new configuration is 22.6% (25.4% without the skull) and the Beam overlap parameter is around 34% (68.9% without the skull). Overall, the targeting properties (Target overlap parameter) are very similar in the presence of the skull and thus prototyping in water can thus be useful. Standing waves are visible in figure 5.a, more precisely between the skull and the transducer, but also within the brain near to the skull.

B. Optimization of the SEFT focusing

Simulations with the MIDA human head model show that the Beam overlap parameter is less than 35 % (Table IV). In order to increase the volume fraction of the beam above half of the peak pressure that falls inside the STN region and to avoid interaction with the adjacent tissues, an adapted SEFT model was designed and simulated with the MIDA human model. This adapted SEFT transducer still has a center frequency of 0.5 MHz, but with an altered curvature radius of 125 mm and an aperture width of 130 mm. The position of the adapted SEFT design was slightly moved to ensure focusing at the STN region (4 mm increase in the SEFT-head distance along the beam axis). A pressure amplitude of 1.97 kPa on the transducer's surface was imposed to reach the target value of 100.21 W/m^2 in the STN region. The simulations (Table V) predict an increase of 44.8% in the Beam overlap parameter, thus exhibiting a better focusing and less potential stimulation of adjacent tissues. The adapted SEFT results in a decrease in the volume of the STN reaching half maximum intensity (decrease of 10.6 % in the Target overlap parameter). This adapted SEFT transducer will be used for the sensitivity analysis in the remainder of this work.

C. Sensitivity analysis of the skull acoustic properties

In a few studies, the acoustical properties of the human skull have been measured [24, 44, 45]. However, this data showed quite some variation so a sensitivity analysis is justified. Simulations were run using the optimized SEFT (see Section III. B). The basic configuration is with an attenuation coefficient of 81 Np/m, a sound speed of 2300 m/s, and a density of 1912 kgm^{-3}. The skull attenuation coefficient was varied in a range of ±75% (from 20 Np/m to 150 Np/m), the skull sound velocity in a range between 1500 m/s (water) and 3450 m/s. The effect of density was explored in a range of ±10% (from 1720.8 kgm^{-3} to 2103.2 kgm^{-3}). When a specific parameter was varied, the standard values were used for the others.

Figure 6 shows the results of the sensitivity analysis regarding skull acoustic parameters. Upper panels illustrate the influence on the maximum intensity and the maximum pressure, while lower panels show results for the Target overlap and the Beam overlap parameters. Changes in velocity greater than

±10% and in attenuation greater than ±50% result in deterioration of the FWHM region and focus parameter values decrease to zero.

The peak intensity and pressure decrease with increasing values of the skull acoustic parameters. The maximum relative variations for the peak intensity are equal to 28.6%, 56.7% and 12.2% for the attenuation, sound speed and the density, respectively. For the peak pressure, these values become 9.8%, 24.7% and 5.2%, respectively. To obtain a deviation in peak pressure of less than 5%, the attenuation coefficient, sound speed and density must be correct within 28%, 2.1%, and 9%, respectively. To obtain an error in peak intensity of less than 5%, the tolerances are 9.9%, 1.2%, and 4.3%, respectively.

The position of the focus point did not change significantly within the range of the skull parameters in this sensitivity study. The focal shift changed from 1.64 mm to 1.71 mm within the range of skull parameters. The changes in focus parameters were more reflected in the Target overlap and the Beam overlap. The focusing parameters are less sensitive to the skull parameter variations, with a maximum relative variation of 8.9%, 9.9% and 2.5% for the attenuation, sound speed and the density, respectively, for the Target overlap; and 3.7%, 26.2% and 3.1%, respectively, for the Beam overlap. To obtain an error in focusing of less than 5%, the attenuation coefficient and sound speed should not deviate more than 24% and 2.8%, respectively. Changes in the density within ±10% of the standard value will result in an error of less than 3%.

D. ***Sensitivity analysis of the STN and brain acoustic properties***

Figure 7 and 8 summarize the sensitivity analysis of the STN and brain acoustic parameters. The STN basic parameters are an attenuation coefficient of 0.5 Np/m, a sound speed of 1500 m/s, and a density of 1045 kgm^{-3}. The brain (white and grey matter) basic acoustic parameters are 2.76 Np/m, 1552 m/s, and 1046 kgm^{-3}, respectively. These acoustic parameters were varied in a range of ±10%.

Changes in these parameter ranges result in variations of less than 0.6%. The criteria of less than 5% variation in the peak intensity and pressure, as well as regards the focussing parameters, remain respected over the full parameter range considered.

IV. DISCUSSION

Transcranial focused ultrasound is a noninvasive approach for neuromodulation of cortical and deep brain tissues with a wide variety of applications. However, ultrasound procedures for neurostimulation are strongly dependent on a good understanding of ultrasound transducers and transcranial ultrasonic wave propagation. In this work, a state-of-the-art computational physics model and detailed head models were used to design a single-element transducer depositing low-intensity ultrasonic energy in the deep brain, more precisely in the STN region. We used the model to perform a sensitivity analysis on the acoustic brain tissue and skull parameters regarding intracranial fields and STN targeting. To quantify the model response, we characterized the ultrasound beam using half maximum intensity contours and their corresponding parameters namely Target overlap and the Beam overlap. To ensure accurate use of the numerical models, a basic validation test, recreating acoustic ultrasound fields in a water tank, was performed. Simulations agreed with both empirical observations (deviation of less than 9%) and computational results from other numerical models (deviation of less than 1 %).

Investigation of the skull effect showed an attenuation of 85% and 56% (relative to free water propagation) in the peak intensity and peak pressure, respectively. These values are compared to those found in literature (peak intensity attenuation of 81% [14] and peak pressure attenuation of 42%-88% [15]). The Target overlap was, in most of the cases, very similar in absence or presence of the skull. This means that prototyping the focal spot in water is useful before application of the transducer for human deep brain sonication. Future research should then be more focused on homogenizing the acoustic fields within the target volume and avoid stimulation of adjacent tissues (increasing the Beam overlap parameter). The peak position was slightly shifted, relative to free water propagation, with 1.3 mm along the beam axis. For comparison, finger representations in human primary cortex are at least 2 mm spaced, with an average volume in the order of hundreds of mm^3 [46]. Thus, tFUS should be able to resolve finger representations within humans. The existing transducer modeled in this work sonicated only 22.6% of the targeted region with a Beam overlap parameter around 34 %. Adaptations

of this SEFT design at the same frequency of 0.5 MHz lead to a Beam overlap of 61.45% (90.1% without skull).

The impact of accurate mapping of the acoustic medium properties on the intracranial fields was examined using the MIDA head model. A sensitivity analysis was carried out, examining the impact of systematic changes in the assigned sound speed, attenuation coefficient, and medium density. Overestimation of the density, sound speed, and absorption of the human skull leads to a corresponding decrease in the simulated transcranial ultrasound fields, and vice versa. This is due to the increased acoustic absorption and impedance, resulting in increased attenuation. The peak pressure was less sensitive to variations in the medium properties than the peak intensity (since intensity is proportional to the second power of pressure). The peak intracranial intensity and pressure are thus affected by the values of sound speed, density, and attenuation coefficient. Their impact is less important on focusing parameters. The intracranial fields are most dramatically affected by changes in sound speed, while changes in density and absorption have a minor effect only. To obtain less than 5% error in peak intensity (which is the most sensitive intracranial field) and focusing parameters, the sound speed must be known quite accurately. More precisely, this means a deviation smaller than 1.2% (or ±28 s/m). The attenuation coefficient must be known with less than 9.9% error (or 8 Np/m) to achieve this accuracy. Density has a significant effect on intracranial fields only, and a change of less than 4.3% (or ±82 kgm^{-3}) is required to obtain less than 5% error in peak intensity. Changes in the STN and brain acoustic parameters in a range of ±10% resulted in only small effect on both the intracranial acoustic fields and the focusing parameters (errors less than 5 %). In this analysis, skull thickness was not considered. The effect of inter-personal skull thickness was shown to be relevant in other works [47]. Most research suggests that personalized tuning of equipment (which would mean here personalized curvature of the SEFT) might be needed for optimal sonication. Various applications can be found where the phases of multi-element arrays were adjusted to the subject's skull structure (based on numerical simulations and using CT scans of the skull) [15]. Also relevant are the simulations in [47] using a simple curved layer of homogeneous bone tissue taken from the surface of a sphere [47]. They show that changes in skull thickness can result in an error in peak pressure greater

than 5%. However, such findings with a simplified spherical model of the human skull would need to be scaled and adjusted to a more realistic heterogonous skull model.

To place this work in context, Mueller et al [14] investigated the effect of changes in some brain tissue models using a spherical homogeneous skull model. Based on their simulations, it was concluded that dedicated brain tissue acoustic parameters were of limited importance (based on a spherical homogeneous skull model), but large changes in sound speed and density of the brain tissue (scaling by a factor two or more) did have a significant effect. They also observed a reduction in the peak RMS intensity by 40% when changing skull geometry from flat to curved, supporting the results of the present work on the importance of geometry, and generally affirmed that the skull was the major material influence on the intracranial field. They also investigated the effect of considering the skull as a homogenous medium with consistent bulk properties and concluded that simplifying the skull by assigning homogenous properties may be sufficient for some skull models with regard to the position of peak pressures and the FWHM volume. This seems to work with a female (small) skull model, but not necessarily for all skull geometries: the male skull model resulted in larger changes in the FWHM volume and location of peak pressure [48]. In [49], authors showed the impact of the acoustic properties of the skull on the predicted temperature elevation. Similar to our study, the paper emphasizes the importance of the skull acoustical parameters for the size of the targeted focal spot. Robertson et al. [47] performed a sensitivity analysis of the transcranial ultrasound fields to acoustic medium properties (sound speed, absorption, density and skull thickness) using a SEFT and a homogeneous spherical skull model. Results in [48] showed that sound speed is the most influential acoustical property, and must be defined with less than 4% error to obtain acceptable accuracy (variations less than 5% in the intracranial fields) in simulated focus pressure, position, and volume, supporting results of the present study. Changes in the skull thickness as small as 0.1 mm can result in peak intracranial pressure error exceeding 5%, confirmed also in [47]. Results of the present study show that the intracranial fields are more sensitive compared to those of Robertson et al. [47]. This is due to the fact that in [47], the used metric is the peak pressure instead of the peak intensity as used in our study. Secondly, the head model used in [47] is homogeneous and spherical, which is less detailed

than the MIDA human model used here. This leads to larger changes in the fields and the focusing parameters, as also pointed at by Mueller et al. in [48].

A more detailed analysis of the pressure field distribution inside the brain and near the head shows the presence of standing waves upon sonication. However, their impact in the current application is expected to be very limited: intensities at the anti-nodes of the modal structure are significantly smaller than in the focal region itself, while energy deposition is low anyhow. In addition, there are signal processing techniques available to mitigate such modes [33, 34] to further exclude their impact.

Finally, results from literature dealing with brain tissue thermal effects show that the temperature increase will be negligible at this low intensity acoustic energy [14, 38, 46]. For example, in [14], the greatest temperature increases observed as a result of applying ultrasound were seen in the skull itself, amounting to a 0.16°C increase. Inside the brain, the predicted temperature increase was only 4.27 10^{-3} °C [14]. Such small changes in tissue temperature can be considered negligible. Note that those values are for an intracranial intensity of around 60 kW/m^2, which is at least two orders of magnitude higher than the intensity aimed at in this work.

A potential limitation of this work is the extent to which the results are generalizable. The sensitivity analysis was carried out with a specific single element transducer and highly detailed but specific skull geometry (MIDA). The location of the STN inside the human head can change between persons and thus the target location may need to be adapted. Different strategies can be used for the localization of the STN structure as reported in the literature [15]. Average coordinates and orientation of the STN over a population could be used, and thus corrections can also be applied for each head size, if necessary. Since most of Alzheimer's and Parkinson's patients underwent MRI, a realistic STN segmentation can be obtained for each subject to find the structure and then plan for the best sonication path. MRI guidance can also be used to compensate the focus displacement and provide better focusing and STN targeting.

The detailed numerical simulations performed in this work showed that a simple SEFT has the potential to deposit ultrasonic energy at a deep brain structure like the STN. The use of such a single

element transducer could be an alternative to the well-established practice of multi-element phased arrays. Note that in both cases, designs might be adopted to the person insonicated. This can be by either changing the reflector shape and/or positioning relative to the skull (when using a SEFT), or by changing the relative phases at the various elements (when using multi-element transducers). A full comparison between both types is beyond the scope of the current paper.

Translation of the acoustic energy to neuron stimulation is clearly beyond the scope of this work; this study showed that acoustic energy can be deposited transcranially to the targeted region of the STN without impacting nearby brain tissues. However, numerical work by Tharnaud et al. [50] suggests that stimulation in human STN by ultrasound would be possible. This transcranial focused ultrasound thus seems an alternative for conventional deep brain stimulation, because of its theoretical ability to modulate deep brain nuclei non-invasively and selectively. However, the therapeutical potential of human ultrasonic subthalamic nucleus stimulation is still elusive, as no experimental studies have been performed [50].

REFERENCES

[1] C. Oluigbo, A. Salma, and A. Rezai, "Deep brain stimulation for neurological disorders," IEEE Rev. Biomed. Eng., vol. 5, pp. 88–99, 2012.

[2] J. O'Shea and V. Walsh, "Transcranial magnetic stimulation: a primer.," Neuron, vol. 55, no. 2, pp. 187–199, 2007.

[3] M. A. Nitsche, L. G. Cohen, E. M. Wassermann, A. Priori, N. Lang, A. Antal, W. Paulus, F. Hummel, P. S. Boggio, F. Fregni, and A. Pascual-Leone, "Transcranial direct current stimulation: State of the art 2008 32," Brain Stimul., vol. 1, no. 1935–861X (Print), pp. 206–223, 2008.

[4] Y. Tufail, A. Matyushov, N. Baldwin, M. L. Tauchmann, J. Georges, A. Yoshihiro, S. I. H. Tillery, and W. J. Tyler, "Transcranial Pulsed Ultrasound Stimulates Intact Brain Circuits," Neuron, vol. 66, no. 5, pp. 681–694, 2010.

[5] T. Deffieux, Y. Younan, N. Wattiez, M. Tanter, P. Pouget, and J. F. Aubry, "Low-intensity focused ultrasound modulates monkey visuomotor behavior," Curr. Biol., vol. 23, no. 23, pp. 2430–2433, 2013.

[6] W. Lee, H.-C. Kim, Y. Jung, Y. A. Chung, I.-U. Song, J.-H. Lee, and S.-S. Yoo, "Transcranial focused ultrasound stimulation of human primary visual cortex," Sci. Rep., vol. 6, no. 1, p. 34026, 2016.

[7] W. Legon, L. Ai, P. Bansal, and J. K. Mueller, "Neuromodulation with single-element transcranial focused ultrasound in human thalamus," Hum. Brain Mapp., vol. 39, no. 5, pp. 1995–2006, 2018.

[8] J. Mueller, W. Legon, A. Opitz, T. F. Sato, and W. J. Tyler, "Transcranial focused ultrasound modulates intrinsic and evoked EEG dynamics," Brain Stimul., vol. 7, no. 6, pp. 900–908, 2014.

[9] O. Naor, Y. Hertzberg, E. Zemel, K. Hynynen, R. M. Jones-, N. Mcdannold, M. Livingstone, A. Opitz, W. J. Tyler, M. Fini, S. Krupa, and S. Shoham, "Ultrasonic neuromodulation," J. Neural Eng., vol. 13, 2016.

[10] N. Lipsman, M. L. Schwartz, Y. Huang, L. Lee, T. Sankar, M. Chapman, K. Hynynen, and A. M. Lozano, "MR-guided focused ultrasound thalamotomy for essential tremor: A proof-of-concept study," Lancet Neurol., vol. 12, no. 5, pp. 462–468, 2013.

[11] R. Bauer, E. Martin, S. Haegele-Link, G. Kaegi, M. von Specht, and B. Werner, "Noninvasive functional neurosurgery using transcranial MR imaging-guided focused ultrasound," Park. Relat. Disord., vol. 20, no. SUPPL.1, 2014.

[12] H. Baek, K. J. Pahk, and H. Kim, "A review of low-intensity focused ultrasound for neuromodulation," Biomed. Eng. Lett., vol. 7, no. 2, pp. 135–142, 2017.

[13] A. Bystritsky, A. S. Korb, P. K. Douglas, M. S. Cohen, W. P. Melega, A. P. Mulgaonkar, A. Desalles, B. K. Min, and S. S. Yoo, "A review of low-intensity focused ultrasound pulsation," Brain Stimul., vol. 4, no. 3, pp. 125–136, 2011.

[14] J. K. Mueller, L. Ai, P. Bansal, and W. Legon, "Computational exploration of wave propagation and heating from transcranial focused ultrasound for neuromodulation," J. Neural Eng., vol. 13, no. 5, 2016.

[15] T. Deffieux and E. Konofagou, "Numerical study of a simple transcranial focused ultrasound system applied to blood-brain barrier opening," IEEE Trans. Ultrason. Ferroelectr. Freq. Control, vol. 57, no. 12, pp. 2637–2653, 2010.

[16] V.K. Khanna, "Deep brain stimulation", Implantable Medical Electronics. Springer, 2016, pp. 309-329.

[17] K. Sugiyama, "Complications of deep brain stimulation ", Deep Brain Stimulation for Neurological Disorders. Springer, 2015, pp. 195-206.

[18] R. L. King, J. R. Brown, and K. B. Pauly, "Localization of ultrasound-induced invivo neurostimulation in the mouse model," Ultrasound Med. Biol., vol. 40, no. 7, pp. 1512–1522, 2014.

[19] W. J. Elias, D. Huss, T. Voss, J. Loomba, M. Khaled, E. Zadicario, R. C. Frysinger, S. a Sperling, S. Wylie, S. J. Monteith, J. Druzgal, B. B. Shah, M. Harrison, and M. Wintermark, "A pilot study of focused ultrasound thalamotomy for essential tremor.," N. Engl. J. Med., 2013.

[20] H. Kim, A. Chiu, S. D. Lee, K. Fischer, and S. S. Yoo, "Focused ultrasound-mediated non-invasive brain stimulation: Examination of sonication parameters," Brain Stimul., vol. 7, no. 5, pp. 748–756, 2014.

[21] W. Lee, S. D. Lee, M. Y. Park, L. Foley, E. Purcell-Estabrook, H. Kim, K. Fischer, L. S. Maeng, and S. S. Yoo, "Image-Guided Focused Ultrasound-Mediated Regional Brain Stimulation in Sheep," Ultrasound Med. Biol., 2016.

[22] J. Jagannathan, N. T. Sanghvi, L. A. Crum, C.-P. Yen, R. Medel, A. S. Dumont, J. P. Sheehan, L. Steiner, F. Jolesz, and N. F. Kassell, "High-intensity focused ultrasound surgery of the brain: part 1--A historical perspective with modern applications.," Neurosurgery, 2009.

[23] M. Lu, M. Wan, F. Xu, X. Wang, and X. Chang, "Design and experiment of 256-element ultrasound phased array for noninvasive focused ultrasound surgery," Ultrasonics, 2006.

[24] F. J. Fry and J. E. Barger, "Acoustical properties of the human skull," J. Acoust. Soc. Am., 1978.

[25] M. I. Iacono, E. Neufeld, E. Akinnagbe, K. Bower, J. Wolf, I. V. Oikonomidis, D. Sharma, B. Lloyd, B. J. Wilm, M. Wyss, K. P. Pruessmann, A. Jakab, N. Makris, E. D. Cohen, N. Kuster, W. Kainz, and L. M. Angelone, "MIDA: A multimodal imaging-based detailed anatomical model of the human head and neck," PLoS One, 2015.

[26] Sim4Life, Zurich Med Tech, www.zurichmedtech.com/sim4life/, visited on Octobre 2018.

[27] K. Foote, "Parametric acoustic array and P. J. Westervelt: A tribute. J Acoust Soc Am 2006;119:3232.

[28] C. I. Christov, P. M. Jordan. "Modeling weakly nonlinear acoustic wave propagation". Q J Mech Appl Math, vol. 60, pp. 473–495, 2007.

[29] A. Kyriakou, E. Neufeld, B. Werner, G. Székely, and N. Kuster, "Full-wave acoustic and thermal modeling of transcranial ultrasound propagation and investigation of skull-induced aberration correction techniques: A feasibility study," J. Ther. Ultrasound, vol. 3, no. 1, pp. 1–18, 2015.

[30] R. Narumi, K. Matsuki, S. Mitarai, T. Azuma, and K. Okita, "Focus Control Aided by Numerical Simulation in Heterogeneous Media for High-Intensity," Jpn. J. Appl. Phys., vol. 52, 2013.

[31] J. L. B. Robertson, B. T. Cox, J. Jaros, and B. E. Treeby, "Accurate simulation of transcranial ultrasound propagation for ultrasonic neuromodulation and stimulation," J. Acoust. Soc. Am., vol. 141, no. 3, pp. 1726–1738, 2017.

[32] F. J. Fry, "Transkull transmission of an intense focused ultrasonic beam," Ultrasound Med. Biol., 1977.

[33] P. P. Ye, J. R. Brown, and K. B. Pauly, "Frequency dependence of ultrasound neurostimulation in the mouse brain," Ultrasound Med. Biol., vol. 42, no. 7, pp. 1512–1530, 2016.

[34] S. C. Tang and G. T. Clement, "Standing-wave suppression for transcranial ultrasound by random modulation," IEEE Trans. Biomed. Eng., 2010.

[35] J. Sun and K. Hynynen, “Focusing of therapeutic ultrasound through a human skull: A numerical study,” J. Acoust. Soc. Am., 1998.

[36] K. Hynynen and F. A. Jolesz, “Demonstration of potential noninvasive ultrasound brain therapy through an intact skull,” Ultrasound Med. Biol., 1998.

[37] S. Pichardo, V. W. Sin, and K. Hynynen, “Multi-frequency characterization of the speed of sound and attenuation coefficient for longitudinal transmission of freshly excised human skulls,” Phys. Med. Biol., 2011.

[38] A. Pulkkinen, Y. Huang, J. Song, and K. Hynynen, “Simulations and measurements of transcranial low-frequency ultrasound therapy: Skull-base heating and effective area of treatment,” Phys. Med. Biol., 2011.

[39] S. A. Goss, R. L. Johnston, and F. Dunn, “Compilation of empirical ultrasonic properties of mammalian tissues. II,” J. Acoust. Soc. Am., 1980.

[40] I. Mavridis, E. Boviatsis, and S. Anagnostopoulou, “Anatomy of the Human Subthalamic Nucleus: A Combined Morphometric Study,” Anat. Res. Int., vol. 2013, pp. 1–8, 2013.

[41] B. Howell and C. C. McIntyre, “Role of Soft-Tissue Heterogeneity in Computational Models of Deep Brain Stimulation,” Brain Stimul., 2017.

[42] Hasgall PA, Di Gennaro F, Baumgartner C, Neufeld E, Lloyd B, Gosselin MC, Payne D, Klingenböck A, Kuster N, “IT’IS Database for thermal and electromagnetic parameters of biological tissues,” Version 4.0, May 15, 2018, DOI: 10.13099/VIP21000-04-0. itis.swiss/database

[43] J. L. Robertson, B. T. Cox, and B. E. Treeby, “Quantifying numerical errors in the simulation of transcranial ultrasound using pseudospectral methods,” IEEE Int. Ultrason. Symp. IUS, pp. 2000–2003, 2014.

[44] G. T. Clement and K. Hynynen, “Correlation of ultrasound phase with physical skull properties,” Ultrasound Med. Biol., 2002.

[45] R. M. Jones and K. Hynynen, “Comparison of analytical and numerical approaches for CT-based aberration correction in transcranial passive acoustic imaging,” Phys. Med. Biol., 2016.

[46] P. Dechent and J. Frahm, “Functional somatotopy of finger representations in human primary motor cortex,” Hum Brain Mapp, 2003.

[47] J. Robertson, E. Martin, B. Cox, and B. E. Treeby, “Sensitivity of simulated transcranial ultrasound fields to acoustic medium property maps,” Phys. Med. Biol., vol. 62, no. 7, pp. 2559–2580, 2017.

[48] J. K. Mueller, L. Ai, P. Bansal, and W. Legon, “Numerical evaluation of the skull for human neuromodulation with transcranial focused ultrasound,” J. Neural Eng., vol. 14, no. 6, 2017.

[49] A. Pulkkinen, B. Werner, E. Martin E, et al. "Numerical simulations of clinical focused ultrasound functional neurosurgery". Phys. Med. Biol. 59: 1679-1700, 2014.

[50] T. Tarnaud, W. Joseph, L. Martens and E. Tanghe, "computational modeling of ultrasonic subthalamic nucleus stimulation," in IEEE Transactions on Biomedical Engineering. doi: 10.1109/TBME.2018.2869042.

Table I: Standard acoustic material properties of head tissues used in this work.

Material	Sound speed (m/s)	Density (kg.m^{-3})	Specific acoustic impedance (MPa s/m)	Attenuation coefficient (Np/m)
Water	1483	999.5	1.5	0.02
Skull (inner table)	2300	1912	4.4	81
Skull (outer table)	2300	1875	4.3	81
Skull (diploe)	2013	1740	3.5	60.8
STN	1500	1045	1.5	0.50
Brain	1552	1046	1.6	2.76

Table II: SEFT parameters for the free water validation case as described in Ref. [14]

Parameter	Value
Curvature radius	50 mm
Aperture width	30 mm
Operating frequency	0.5 MHz
Medium's speed of sound	1483 m/s
Source amplitude	0.145 MPa
Source phase	0°
Boundary conditions	Perfectly matched layers (absorbing boundary conditions)
Cell size (< λ/10)	0.2 mm

Table III: Quantification of the half maximum intensity profile in free water for the validation case from Ref. [14]

	Experiment	Model (COMSOL) [14]	Model (Sim4Life)
Max pressure (MPa)	0.91	0.83	0.83
Max intensity (W/cm^2)	23.87	23.66	23.45
Major axis (mm)	30.81	28.93	28.96
Minor axis (mm)	3.85	4.28	3.98
Centroid x (mm)	-0.14	0.00	0.00
Centroid y (mm)	8.46	6.84	0.00
Major axis vertical offset (°)	1.23	0.00	0.00

Table IV: FWHM quantification at the (virtual) STN zone in free water and in presence of the MIDA skull model.

	Free water	Non-adjusted intensity (0.81 kPa)	Adjusted intensity (2.1 kPa)
Max intensity (W/m^2)	100.1	15.1	101.55
Max pressure (kPa)	14.58	6.42	16.265
Peak displacement (mm)	---- ----	1.3 axial+ 0.4 lateral	1.9 axial+ 0.5 lateral
Major axis (mm)	17.64	22.9	23.38
Minor axis (mm)	3.4	3.06	3.79
Target overlap (%)	25.4	22.95	22.64
Beam overlap (%)	68.87	36.49	33.92

Table V: FWHM quantification of the adapted SEFT design

	Free water	MIDA
Major axis (mm)	7.95	18.33
Minor axis (mm)	1.84	2.87
Target overlap (%)	24.2	20.23
Beam overlap (%)	90.12	61.45

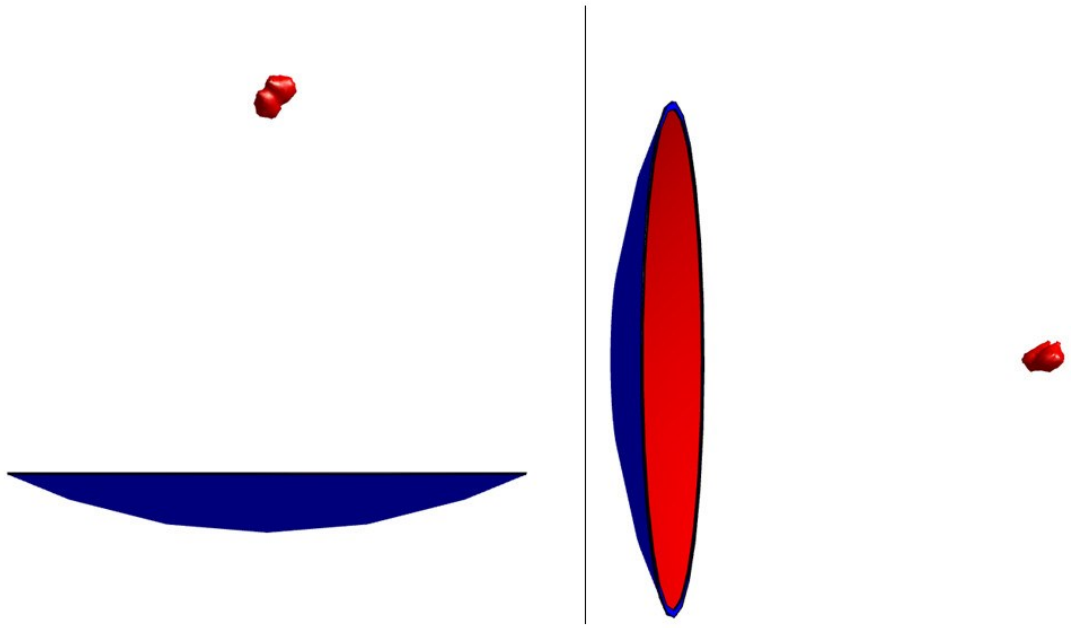

Figure 1: Spherical single-element ultrasound transducer. In red the piezoelectric element is shown and in blue the reflector. The STN is also indicated by the red volume in the center of the drawing.

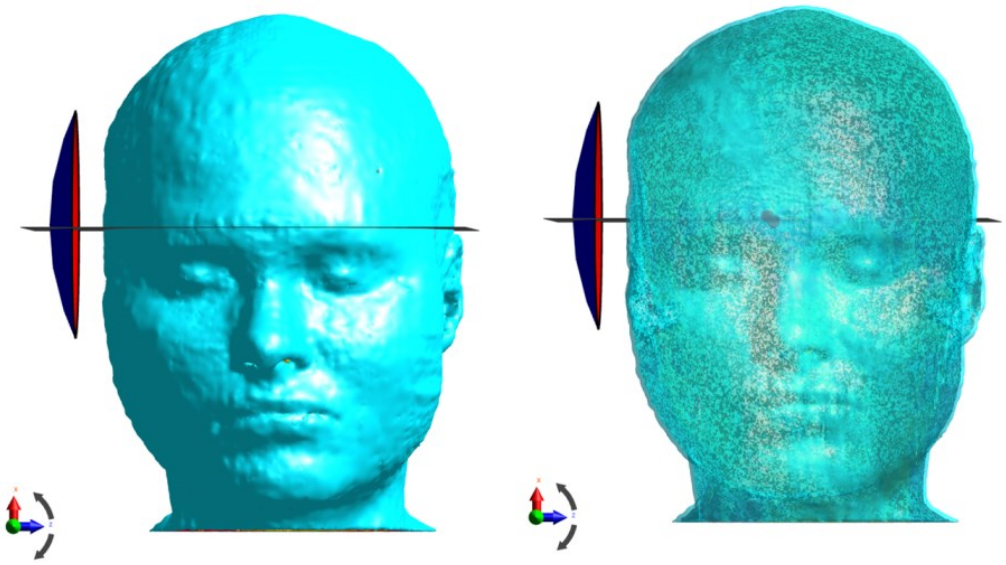

Figure 2: MIDA head model with location of the STN inside the brain.

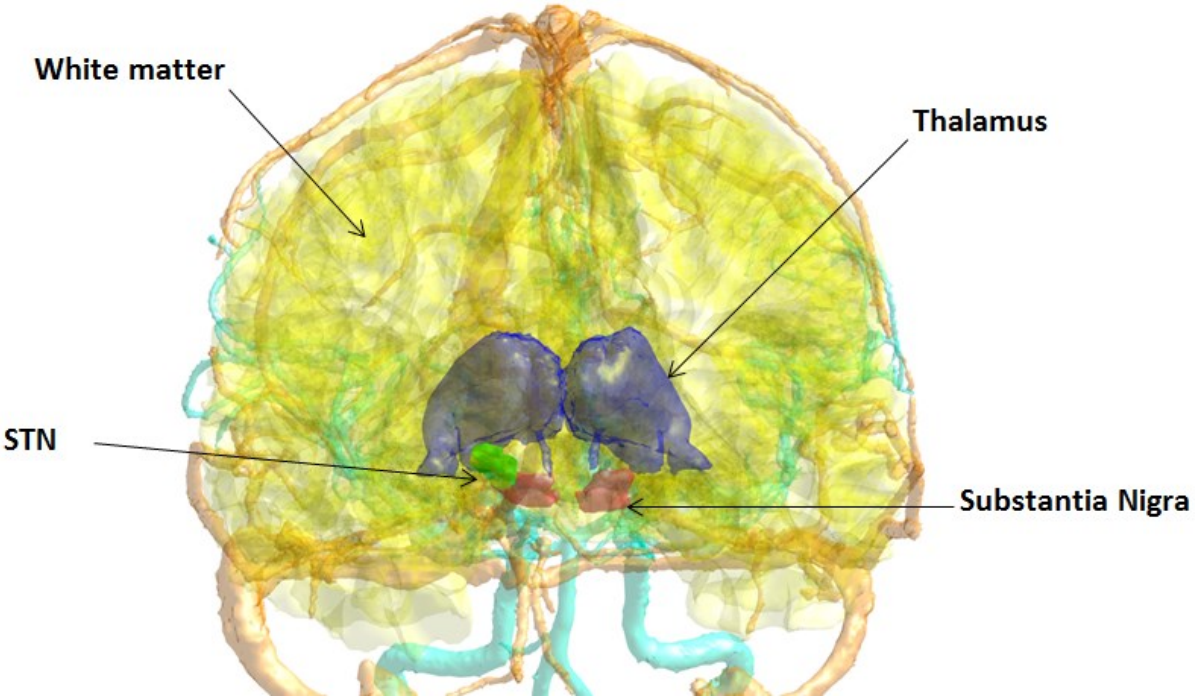

Figure 3: STN modelled in the MIDA human head model

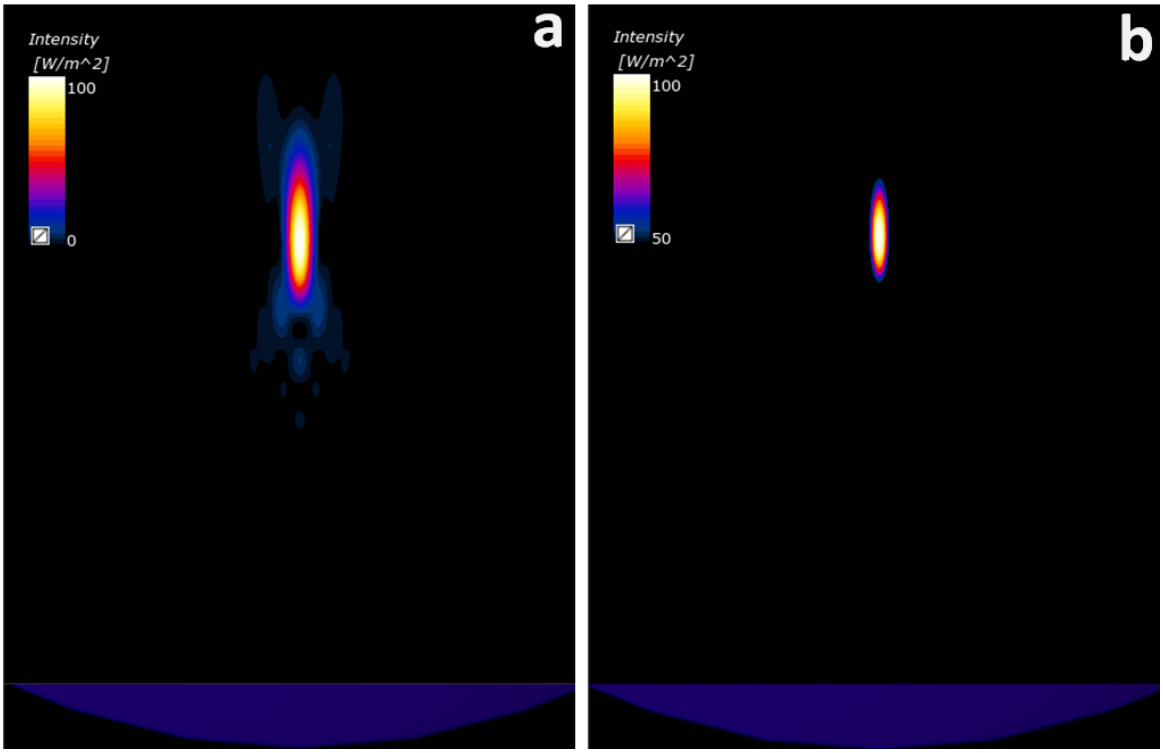

Figure 4: Simulation results depicting the intensity distribution from the SEFT in free water. (a): Intensity distribution in the YZ plane. (b): Half maximum intensity profile.

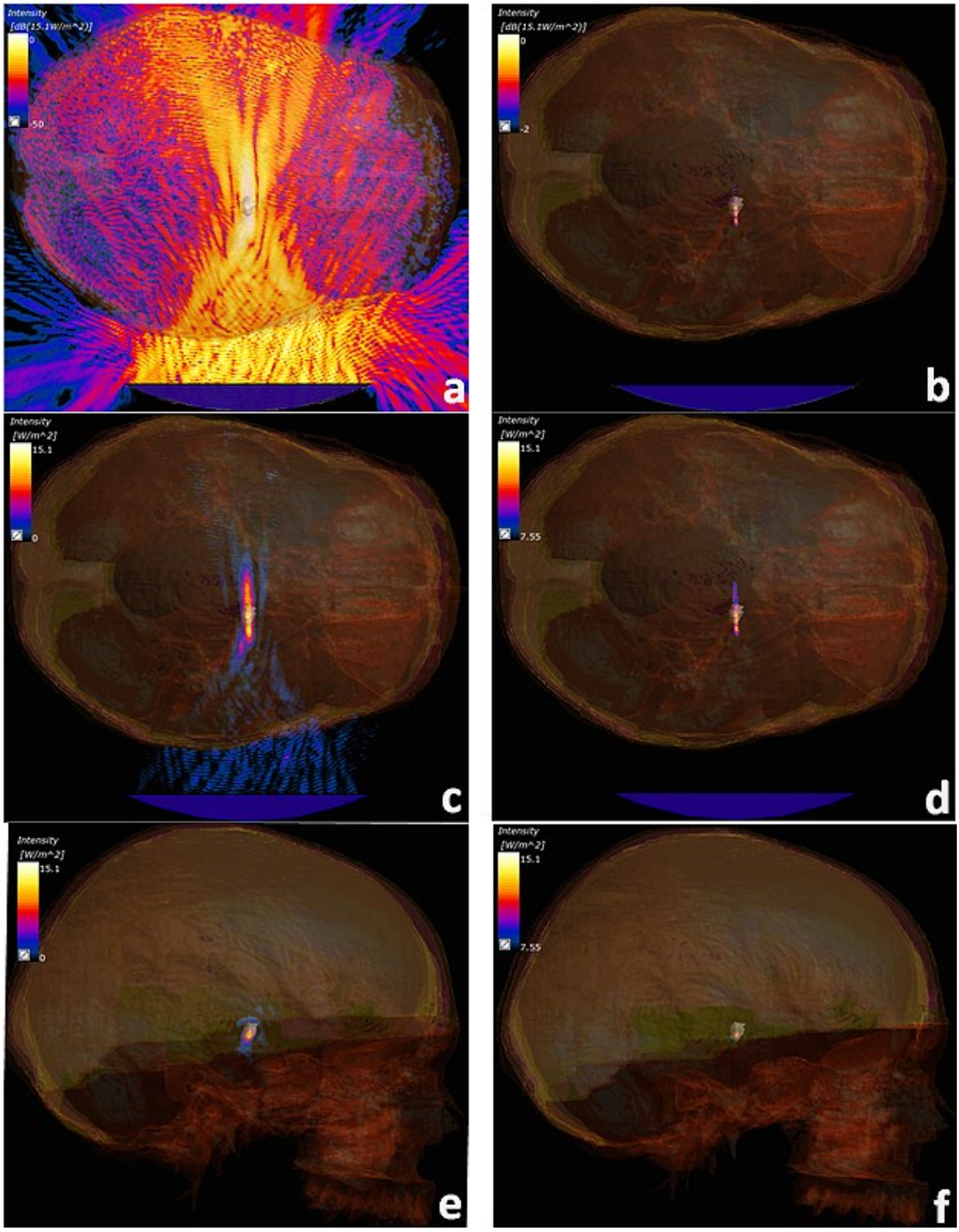

Figure 5: acoustic intensity distribution in the MIDA human skull model (left column) and illustration of the FHWM region (right column). a-b: Intensity distribution in the transverse plane in dB (15.1 W/m^2), from 0 to -50 for (a) and from 0 to -2 for (b). c-d: Intensity distribution in the transverse plane, from 15.1 to 0 for (c) and from 15.1 to 7.55 for (d). e-f: Intensity distribution in the sagittal plane, from 15.1 to 0 for (e) and from 15.1 to 7.55 for (e).

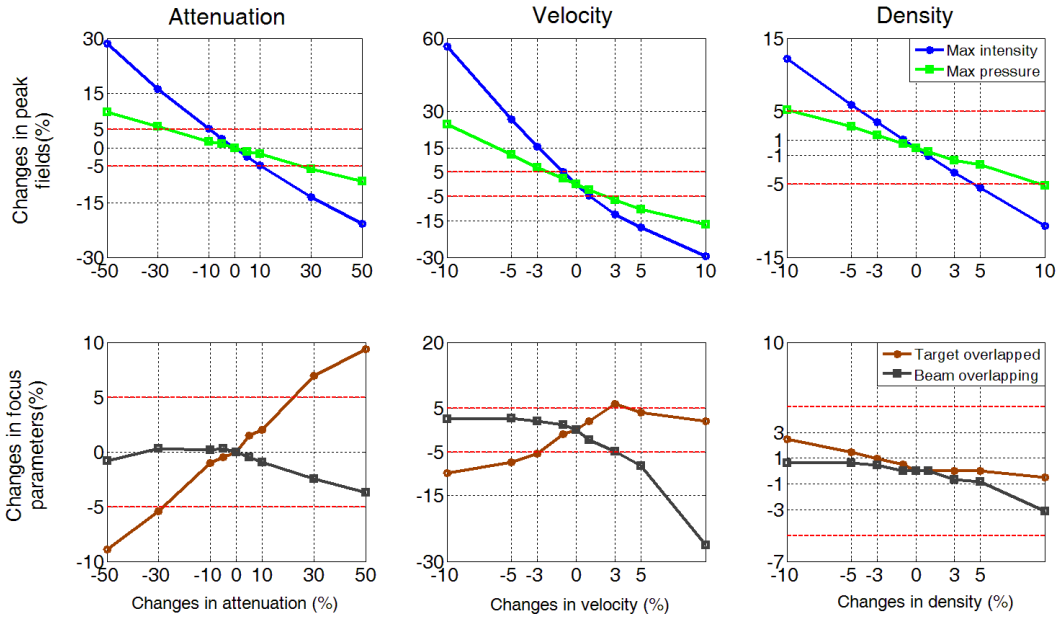

Figure 6: Relative changes in the intracranial fields and focusing parameters when varying the skull acoustic properties. Changes in focus parameters mean changes in the Target overlap and the Beam overlap parameters compared to results for the default configuration (attenuation coefficient of 81 Np/m, a sound speed of 2300 m/s, and a density of 1912 kgm^{-3}).

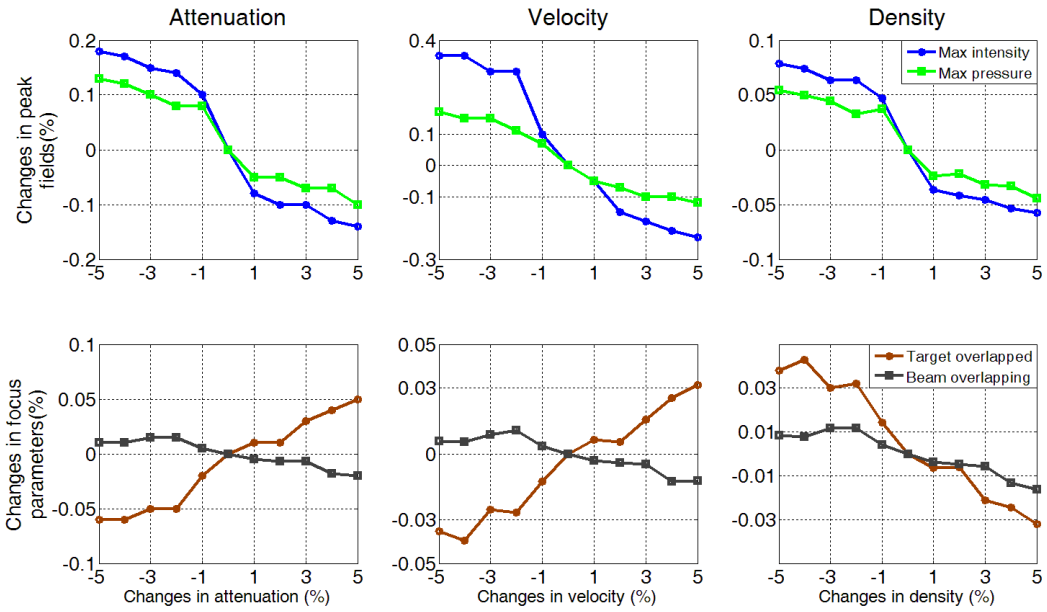

Figure 7: Relative changes in the intracranial fields and focusing parameters when varying the STN acoustic properties. Changes in focus parameters mean changes in the Target overlap and the Beam overlap parameters compared to results for the default configuration (attenuation coefficient of 81 Np/m, a sound speed of 2300 m/s, and a density of 1912 kgm^{-3}).

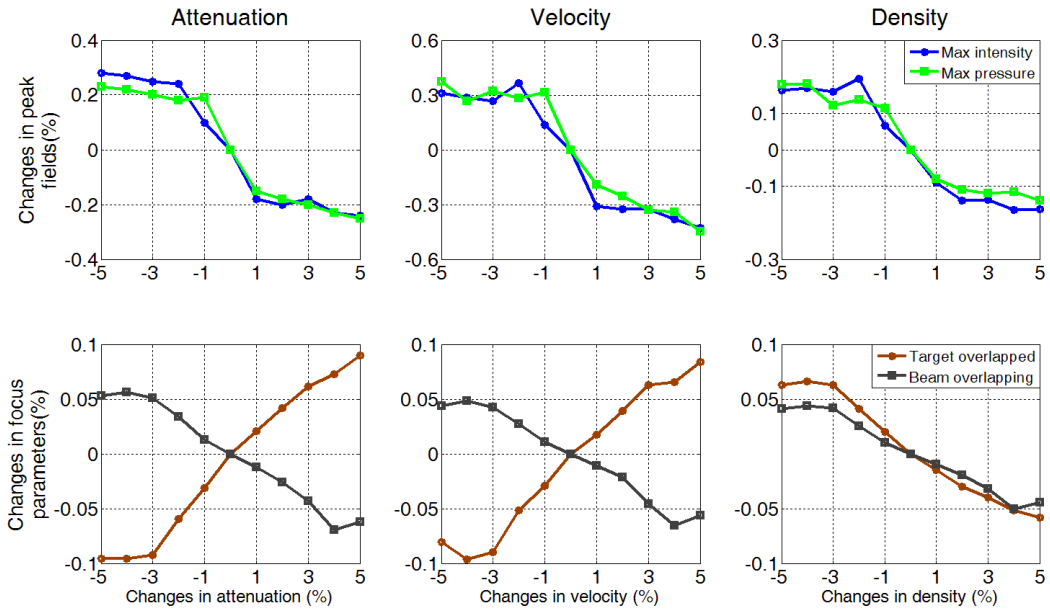

Figure 8: Relative changes in the intracranial fields and focusing parameters when varying the brain (white and grey matter) acoustic properties. Changes in focus parameters mean changes in the Target overlap and the Beam overlap parameters compared to results for the default configuration (attenuation coefficient of 81 Np/m, a sound speed of 2300 m/s, and a density of 1912 kgm^{-3}).